Positron affinities for elemental metals

1989 J. Phys.: Condens. Matter 1 6081

(http://iopscience.iop.org/0953-8984/1/35/008)

J. Phys.: Condens. Matter **1** (1989) 6081–6093. Printed in the UK

Positron affinities for elemental metals

M J Puska, P Lanki and R M Nieminen
Laboratory of Physics, Helsinki University of Technology 02150 Espoo, Finland

Received 30 January 1989, in final form 21 April 1989

Abstract. The relevant quantity in the comparison of the absolute positron energy levels in different materials is the sum of the internal electron and positron chemical potentials, i.e. the sum of the Fermi level and the bottom of the lowest positron band relative to a common, well-defined reference energy. This sum is defined as the positron affinity. The positron affinity reflects the preference of the positron for different components in heterostructures made of different materials and the preference between the host matrix and precipitates in alloys. Moreover, the affinity is closely related to the positron work function and positronium formation potential which are important parameters in the slow-positron-beam experiments. We have determined the positron affinity for the alkaline and alkaline-earth metals, 3d-, 4d-, and 5d-transition metal series, and for some metals on the right in the Periodic Table. The diamond structure semiconductors are also considered. The determination is based on the self-consistent electron structure calculations and the subsequent calculation of the positron band structure within the local-density approximation. The trends are studied and interpreted along the different columns and rows of the Periodic Table. The results are also compared with available experiments.

1. Introduction

The experimental methods based on positron annihilation have a large number of applications in the different subfields of solid state physics [1, 2]. For example, positron lifetime and Doppler-broadening spectroscopies have been extensively used to study defects in crystal structures. The angular correlation techniques are capable of determining Fermi-surface topologies. The properties of solid surfaces and the near-surface regions have recently been investigated by slow-positron-beam techniques. One of the key prerequisites for the proper interpretation of the experimental results is the understanding of the properties of delocalised positrons in perfect lattices. These kinds of properties include the positron energetics, i.e. the positron energy level relative to the vacuum, and its variation in a solid between regions of different structure or chemical composition. The positron diffusion properties also belong to this category.

The relative positions of the energy levels of delocalised positrons between different materials in contact are determined by one number, the positron affinity. We define it as the sum of the internal electron and positron chemical potentials. The electron part takes care of the electrostatic energy difference due to the dipole layer near the interface. Note that the positron affinity defined this way will be a *negative* number, and a larger negative value means a stronger preference of the positron in the material in question. Moreover, the affinity gives directly the positronium (Ps) formation potential and,

0953-8984/89/356081 + 13 $02.50

combined with the electron work function, the positron work function with respect to the vacuum level. These two quantities are very important, directly measurable parameters in slow-positron-beam experiments. Finally, the volume dependence of the positron affinity (the deformation potential) can be used to estimate the positron diffusion constant.

The calculations of this work are based on the density-functional theory in the local-density approximation (LDA) for exchange and correlation [3]. First, the self-consistent electron structures are calculated by the linear-muffin-tin orbital method (LMTO) within the atomic-spheres approximation (ASA) [4, 5]. Thereafter the positron potential is determined within LDA for the electron-positron correlation effects, and the positron wave function and energy eigenvalue are calculated also using LMTO-ASA. The Fermi level and the bottom of the lowest positron band obtained define the internal electron and positron chemical potentials. The great benefit of ASA is a simple absolute energy scale determined by the Coulomb potential due to spherical charge densities of the atomic spheres [6]. In the case of FCC and BCC metals the spheres are in fact neutral. This feature of ASA has also been employed in estimating the electron deformation potentials for semiconductors [7] and the band offsets for semiconductor heterojunctions [6].

The main purpose of this work is to provide a consistent positron affinity data base including a large number of elemental metals. This data base can be used as a guideline in the interpretation of experimental results. It also enables a fruitful study of different trends seen along the columns and rows of the Periodic Table. Especially, it is interesting to analyse the trends in the positron affinity resulting from the interplay between the electron and positron chemical potentials, which reflect differences in the one-particle potentials and also different aspects of the one-particle band structures. Moreover, the comparison of the theoretical and experimental Ps formation potentials gives an idea about the validity of the approximations (nominally LDA) made. The power of the theoretical method has already been shown in a previous paper [8] based on similar calculations for some metals and semiconductors, but the trends were not studied systematically in that work.

2. Theory

The calculation methods and the theory of the electron and positron energy levels are carefully explained in the previous publication [8]. Therefore we give here only the main points. In the LDA of the density-functional theory the effective potential for the electrons is written in the form

$$v_{eff}(\boldsymbol{r}) = \varphi(\boldsymbol{r}) + v_{xc}(n(\boldsymbol{r})) \tag{1}$$

where $\varphi(\boldsymbol{r})$ is the Coulomb potential due to the nuclei and electron charge density and v_{xc} is the LDA exchange-correlation potential [9], which depends on the electron density $n(\boldsymbol{r})$. The effective potential determines the electron density in turn, and the ensuing self-consistency problem is solved in this work by the LMTO-ASA method. The method gives the electron-band structure, the most important parameter of which for the present application is the Fermi level. The potential sensed by the positron is constructed as

$$V_+(\boldsymbol{r}) = -\varphi(\boldsymbol{r}) + V_{\text{corr}}(n(\boldsymbol{r})) \tag{2}$$

where φ is the same Coulomb potential as in equation (1), and V_{corr} is the correlation

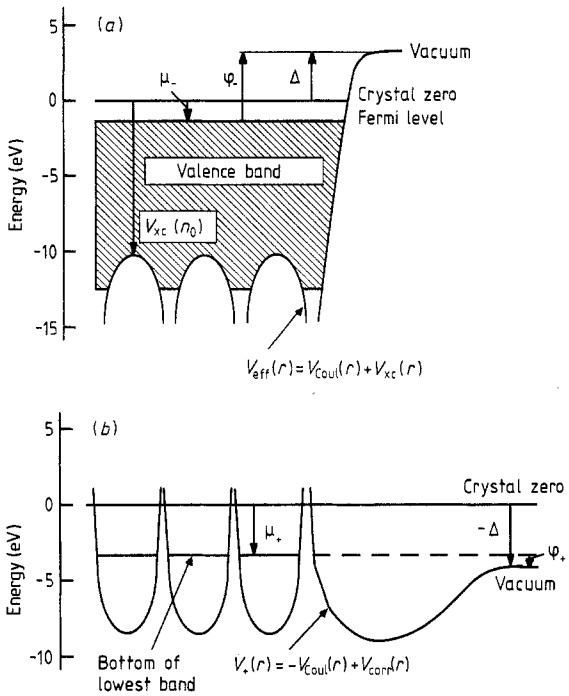

Figure 1. Electron (*a*) and positron (*b*) potentials and energy levels near a metal surface. The vertical scale corresponds to the case of Al. Δ is the dipole potential at the surface, $v_{xc}(n_0)$ is the exchange-correlation potential in the interstitial region, and φ_- and φ_+ denote the electron and positron work functions, respectively. μ_- and μ_+ are the electron and positron chemical potentials, respectively. Arrows pointing upwards and downwards denote positive and negative quantities, respectively.

potential describing the energy lowering due to the electron pile-up near the positron. The correlation potential V_{corr} is treated within LDA based on the many-body calculations for a delocalised positron in a homogeneous electron gas [10]. In the case of semiconductors the correlation effects are slightly reduced reflecting the imperfect screening [11]. The positron band structure is also calculated by the LMTO-ASA method.

In the LMTO-ASA method the potentials and energy levels are given with respect to the so-called crystal zero level, which is defined as the zero of the Coulomb potential due to the nuclei and the electron density of the infinite solid. In the ASA the lattice is divided into spheres centred around nuclei and in the case of diamond-structure semiconductors considered in this work also around the tetrahedral interstitial sites. The spheres fill the whole space and the electron density and the potentials are approximated to be spherical inside these spheres. Therefore the calculation of the Coulomb potential and the determination of the crystal zero is easy. For example, in the case FCC and BCC metals, for which all the spheres are similar neutral Wigner–Seitz spheres, the Coulomb potential due to every sphere vanishes just outside its surface.

The form of the potentials and the different energy levels for electrons and positrons in bulk crystals are shown in figure 1. The vertical scale corresponds the illustrative example of aluminium. The maximum of the effective potential occurs in the interstitial region (in ASA on the surface of the Wigner–Seitz sphere). Because the Coulomb potential vanishes there, the maximum is below the crystal zero by the exchange-correlation potential $v_{xc}(n_0)$ calculated from the interstitial electron density n_0 (the electron density on the surface of the Wigner–Seitz sphere). The valence band width is about 12 eV and the Fermi level is slightly below the crystal zero, so that the chemical potential μ_- is a small negative number. The electron energy levels with respect to vacuum are determined by the potential difference Δ due to the surface dipole charge,

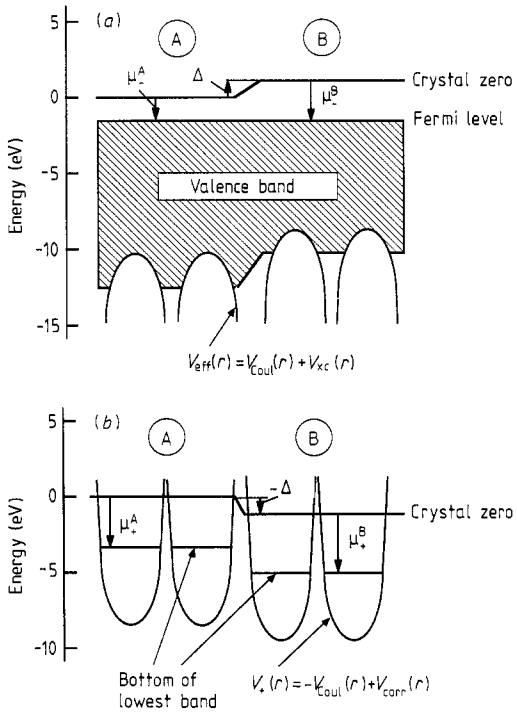

Figure 2. Electron (*a*) and positron (*b*) potentials and energy levels near a junction of two metals. The vertical scale corresponds to an Al-Zn junction. See also the caption to figure 1.

which arises because the electron density of the Wigner–Seitz cells relaxes near the surface from that for a bulk cell. As a result the dipole potential is measured with respect to the crystal zero. The electron work function φ_- is of course the distance from the Fermi level to vacuum. In the case of positrons the minimum of the total potential in bulk occurs in the interstitial region. This minimum is below the crystal zero by the correlation potential $v_{\mathrm{corr}}(n_0)$. The positron chemical potential corresponds to the bottom of the lowest positron energy band, and is about 3 eV below the crystal zero. Outside the surface in vacuum the total positron potential has a wide minimum due to the correlation effects, which further away from the surface form the image potential [2]. The image potential vanishes towards the vacuum level, which is below the crystal zero by the amount of the surface dipole potential Δ. The surface dipole is slightly larger in magnitude than the positron chemical potential, and therefore the positron energy level in bulk is higher than in vacuum, i.e. the positron work function is negative.

Figure 2 shows the behaviour of the energy levels when two different metals are in contact. The vertical scale corresponds to the junction between Al and Zn. The Fermi levels equalise themselves via the formation of an interface dipole with the potential difference $\Delta = \mu_-^{\mathrm{A}} - \mu_-^{\mathrm{B}}$. As a result the difference between the lowest positron energies on the different sides of the interface is given by

$$\Delta E_+^{\mathrm{A,B}} = E_+^{\mathrm{A}} - E_+^{\mathrm{B}} = \mu_-^{\mathrm{A}} - \mu_-^{\mathrm{B}} + \mu_+^{\mathrm{A}} - \mu_+^{\mathrm{B}}. \tag{3}$$

This equation shows that it is useful to define the positron affinity as the sum

$$A_+ = \mu_- + \mu_+. \tag{4}$$

A_+ is then a specific bulk property for every material. As a consequence the difference

of the positron energies between materials in contact is the difference in the positron affinities.

The important quantities measured in slow-positron-beam experiments [2] are also related to the positron affinity. The positronium formation potential ε_{Ps} is defined as the negative of maximum kinetic energy of Ps atoms ejected into vacuum from the sample. Ps is not stable in bulk metals or semiconductors, but is formed near the surface when a delocalised positron is leaving the solid. The principle of energy conservation gives

$$\varepsilon_{Ps} = \varphi_- + \varphi_+ - 6.8\,\text{eV} \tag{5}$$

because the extraction of a thermalised positron and a Fermi level electron cost in energy the sum of the work functions, but at the same time the Ps binding energy of 6.8 eV is gained. According to figure 1 we can further write

$$\begin{aligned}\varepsilon_{Ps} &= (-\mu_- + \Delta) + (-\mu_+ - \Delta) - 6.8\,\text{eV} \\ &= -A_+ - 6.8\,\text{eV}.\end{aligned} \tag{6}$$

The positron work function φ_+ is another important experimental quantity. It depends on the surface via the surface dipole potential. Its *ab-initio* determination would thus require the calculation of the self-consistent electron density for the surface. However, we can eliminate D by using the experimental electron work function φ_- as

$$\varphi_+ = -\mu_+ - \Delta = -\mu_+ - \mu_- - \varphi_- = -A_+ - \varphi_-. \tag{7}$$

Thus also the positron work function can be expresed in terms of the positron affinity A_+.

The positron diffusion constant D in a perfect solid is determined by scattering from longitudinal acoustical phonons [12]. D depends on the strength of the positron–phonon interaction which can be described by the deformation potential E_d [13]:

$$D = \left(\frac{8\pi}{9}\right)^{1/2} \frac{\hbar^4 \langle c_{ii} \rangle}{(m^*)^{5/2}(k_B T)^{1/2} E_d^2} \tag{8}$$

where m^* is the positron effective mass, T the absolute temperature, and $\langle c_{ii} \rangle$ the elastic constant associated with longitudinal waves and averaged over the directions of propagation. The deformation potential describes the relative change of the positron energy level due to small variations (a phonon) of the atomic density in the bulk and is defined as

$$E_d^+ = V \frac{\partial E_+}{\partial V} \tag{9}$$

where E_+ is the positron energy level, which is measured e.g. with respect to the crystal zero of the undeformed lattice. During the density variations small charge transfers induce potentials which oppose the changes in the internal chemical potential for electrons and balance the Fermi level into a unique value in the whole sample. These induced potentials affect also on the positron energy level in the same way as in figure 2 for two types of metals in contact. As a result, the deformation potential can be calculated as

$$E_d^+ = V \frac{\partial(\mu_+ + \mu_-)}{\partial V} = V \frac{\partial A_+}{\partial V}. \tag{10}$$

Thus it depends on the volume derivative of the positron affinity.

Li bcc 3.247	Be fcc 2.359													
Na bcc 3.883	Mg fcc 3.346												Al fcc 2.992	Si dia 3.183
K bcc 4.862	Ca fcc 4.122	Sc fcc 3.427	Ti fcc 3.052	V bcc 2.818	Cr bcc 2.684	Mn fcc 2.699	Fe bcc 2.662	Co fcc 2.621	Ni fcc 2.602	Cu fcc 2.669	Zn fcc 2.899			Ge dia 3.318
Rb bcc 5.197	Sr fcc 4.494	Y fcc 3.761	Zr fcc 3.347	Nb bcc 3.071	Mo bcc 2.992	Tc fcc 2.840	Ru fcc 2.791	Rh fcc 2.809	Pd fcc 2.873	Ag fcc 3.005	Cd fcc 3.265			Sn dia 3.805
Cs bcc 5.656	Ba bcc 4.652	Lu fcc 3.624	Hf fcc 3.301	Ta bcc 3.069	W bcc 2.945	Re fcc 2.872	Os fcc 2.825	Ir fcc 2.835	Pt fcc 2.897	Au fcc 3.002				Pb fcc 3.657

Figure 3. Lattice structures and Wigner–Seitz radii (in a_0) used in the calculations.

3. Results and discussion

The crystal structures and the Wigner–Seitz radii used in the calculations are shown in figure 3. The Wigner–Seitz radii correspond to the room temperature. For convenience of calculation, the hexagonal structures were approximated by FCC with the same atomic density. We do not expect this substitution to affect strongly the calculated electron and positron chemical potentials, especially in cases when the c/a-value of the hexagonal structure is close to the ideal one. This approximation is also used in some previous works [15] in which the cohesive properties of transition metals have been studied.

The calculated chemical potentials and their volume derivatives in selected cases are given in table 1. The electron data is in agreement with the calculations by Andersen *et al* [4]. The volume dependencies and the ensuing estimates for the diffusion constant have been carefully considered in the previous paper [8], and they are not discussed here. In this paper the emphasis is put on the positron affinity and its trends along the columns and rows of the Periodic Table. The positron affinities are shown in figure 4. It is seen that the affinity is always negative and its magnitude rises from the centre of the transition metal series towards left and right. α-Sn has the largest afinity in magnitude, which reflects the large open interstitial region in the diamond structure. The positron work function and the positronium formation potential would according to equations (6) and (7) have large positive values in the case of α-Sn. Therefore α-Sn is predicted to be for positrons a very efficient trap, from which positrons do not escape as free positrons or as Ps-atoms. The smallest affinity in magnitude is found in the case of the heavy FCC-metal Os. Thus, according to equation (7) Os would have a large negative positron work function, which means that it would be an efficient positron moderator for the slow-positron beams.

The trends of the positron affinity along the 3d-, 4d- or 5d-series can be understood by studying the electron and positron chemical potentials separately. The chemical potentials are shown along the 3d-series in figure 5. In the beginning of the given row bonding d-type orbitals are being filled. As a result, cohesion increases and the Wigner–Seitz radius decreases rapidly. At the same time the electron chemical potential, i.e. the Fermi level, rises because of the filling of the d-levels. The rise of the positron chemical potential is due to decrease of the open interstitial volume seen by the positron. At the

Table 1. Calculated chemical potentials and their volume derivatives for electrons (μ_- and $V(\partial\mu_-/\partial V)$) and positrons ($\mu_+$ and $V(\partial\mu_+/\partial V)$).

Host	μ_- (eV)	μ_+ (eV)	V ∂μ− (eV)	V ∂μ+ (eV)
Li	−2.36	−5.00	−1.67	−0.25
Be	+0.87	−3.98		
Na	−2.32	−4.80	−1.61	−0.98
Mg	−1.89	−4.29	−3.57	−1.07
Al	−0.76	−3.65	−6.02	−1.83
Si	−0.54	−6.41	−7.51	+1.32
K	−2.25	−4.80	−1.23	−1.32
Ca	−2.26	−4.14	−2.66	−1.40
Sc	−1.77	−3.33	−4.96	−1.86
Ti	−1.29	−2.77	−6.64	−2.35
V	−1.01	−2.43	−8.09	−2.24
Cr	−0.35	−2.27	−9.51	−2.49
Mn	−1.15	−2.57	−8.18	−2.51
Fe	−1.16	−2.68	−8.35	−2.47
Co	−1.14	−2.77	−8.36	−2.54
Ni	−1.55	−2.91	−8.13	−2.36
Cu	−1.59	−3.22	−7.39	−2.06
Zn	−1.48	−3.76	−6.123	−1.99
Ge	−0.60	−6.19	−7.64	+1.02
Rb	−2.23	−4.74		
Sr	−2.14	−4.27		
Y	−1.76	−3.55		
Zr	−1.11	−2.87		
Nb	−0.81	−2.12	−9.15	−2.78
Mo	−0.04	−1.88	−11.3	−3.06
Tc	+0.04	−1.71		
Ru	−0.19	−1.73		
Rh	−1.02	−2.08		
Pd	−2.35	−2.69	−9.15	−3.00
Ag	−2.14	−3.22	−7.23	−2.25
Cd	−1.92	−3.86	−5.78	−2.07
Sn	−1.28	−6.32		
Cs	−2.21	−4.73		
Ba	−2.07	−4.06		
Lu	−1.58	−3.32		
Hf	−1.05	−2.65		
Ta	−0.69	−1.94	−9.40	−2.92
W	+0.33	−1.64	−12.0	−3.00
Re	+0.43	−1.40		
Os	+0.44	−1.57		
Ir	+0.04	−1.57		
Pt	−1.37	−2.26	−12.2	−3.00
Au	−1.86	−2.73	−10.2	−3.80
Pb	−1.58	−3.98	−4.81	−1.58

end of the given series antibonding d-type orbitals are being filled causing a decreasing trend in the cohesion and a slight increase in the Wigner–Seitz radius. The electron chemical potential decreases because of the lowering of the centre of the d-bands as a function of the atomic number. The antibonding orbitals are more localised than the

Li -7.36	Be -3.11												
Na -7.12	Mg -6.18											Al -4.41	Si -6.95
K -7.05	Ca -6.40	Sc -5.10	Ti -4.06	V -3.44	Cr -2.62	Mn -3.72	Fe -3.84	Co -4.18	Ni -4.46	Cu -4.81	Zn -5.24		Ge -6.69
Rb -6.98	Sr -6.41	Y -5.31	Zr -3.98	Nb -2.93	Mo -1.92	Tc -1.67	Ru -1.92	Rh -3.10	Pd -5.04	Ag -5.36	Cd -5.78		Sn -7.60
Cs -6.94	Ba -6.13	Lu -4.90	Hf -3.70	Ta -2.63	W -1.31	Re -0.97	Os -0.89	Ir -1.53	Pt -3.63	Au -4.59			Pb -5.56

Figure 4. Calculated positron affinities A_+ (eV).

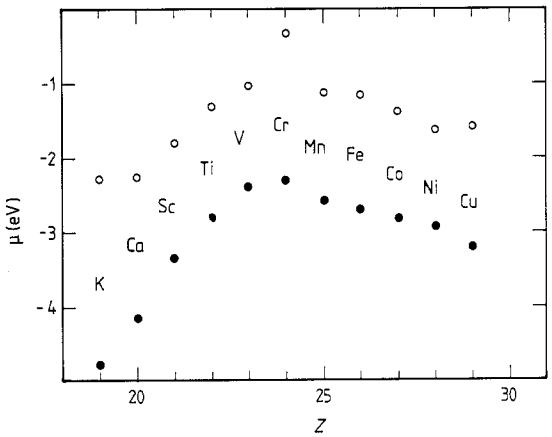

Figure 5. Calculated electron (○) and positron (●) chemical potentials for the 3d-transition metals.

bonding ones. Therefore the screening of the nucleus improves when they are being filled. As a result, the open volume seen by positron increases and the positron chemical potential sinks towards the end of the d-series.

The trends along the columns are also interesting. According to figure 4, within the transition-metal columns in the middle (V-, Cr-, Mn-, Fe-, and Co-columns) the magnitude of the positron affinity decreases monotonically in the downward direction, whereas in the columns on the right (Ni-, and Cu-columns) or on the left (Sc-column) the magnitude of the affinity has maximum in the 4d-series. The separation to electron and positron chemical potentials in the case of V- Cr-, Ni-, and Cu-columns is shown in figure 6. It can be concluded that the maximum of the magnitude of the positron affinity for the Ni- and Cu-columns reflect the drop of the Fermi level. This is connected with the increase of the lattice constant and with the drop of the centre of the d-bands compared to the late 3d-elements. The 4d- and 5d-transition metals, which belong to the same columns, have nearly equal lattice constants. Therefore the Fermi level rises in all cases when going down from the 4d-metal to the adjacent 5d-metal. In the case of the metals belonging to the columns in the middle, the d-bands are being filled and they do not drop when going down from a 3d-metal to the 4d-metal. As a consequence, the Fermi level rises monotonically when going downwards in these columns. The positron chemical potential reflects the changes in open volume seen by the positron. In the sense of the open volume, the increase of the lattice constant between the adjacent 3d- and 4d-elements is compensated by the increase of the core region. The 5d-cores are even

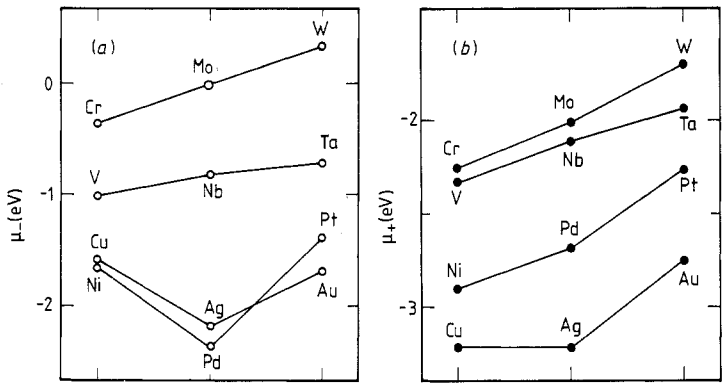

Figure 6. Calculated electron (*a*) and positron (*b*) chemical potentials for the V, Cr, Ni and Cu columns of the Periodic Table.

larger than the 4d-cores. The result is that the positron chemical potential increases monotonically in the downward direction for all transition metal columns. This completes the discussion of the trends in the positron affinity for the transition metals.

The Ps formation potential ε_{Ps} is given by equation (6). According to figure 4 ε_{Ps} is negative for most of the metals, meaning that spontaneous positronium emission is possible, after a thermalised positron has diffused from bulk to the surface. However ε_{Ps} is positive for alkali metals, which means that spontaneous positron emission is not possible there. The theoretical values for the semiconductors Si and Ge are close to zero: spontaneous Ps emission should be possible from Ge but not from Si. The experiments [16, 17] have shown emission from both semiconductors. However, this is not necessarily in disagreement with theory, because surface electron states having energy eigenvalues in the band gap and a large density on the surface can have a strong influence on positronium formation.

The positron affinities have been measured directly for eight different transition metals by Gidley and Frieze [18], who used the reemitted-positron spectroscopy. Their results are copared with the present calculations in figure 7(*a*). For the early BCC metals W, Mo, Ta, and Nb the experimental affinities are slightly larger in magnitude than the theoretical ones, whereas for the late FCC metals Co, Ni, Cu, and Pd the situation is reverse. The discrepancies are less than 1 eV. It is satisfying to note that the experimental and theoretical orderings within the FCC and BCC groups are the same. The positron affinities can be deduced also from the measured positronium formation potentials. This is done in figure 7(*b*), where the results from different sources are compared with the present theoretical values. The agreement is even better than in figure 7(*a*). However, the ordering of Cu and Au is different for theory and experiment.

Slow-positron-beam techniques have been used to study the properties of heterostructures formed by depositing thin metal films on metal substrates [22]. The positron affinities given in figure 3 are very useful numbers for analysing data from these kinds of studies. For example, if a few layers of Cu are evaporated on Ag substrate the positronium emission out of the sample is strongly reduced, whereas an Ag film on Cu does not cause such an effect. These features can be directly predicted from figure 4, because the positron affinity for Ag is 0.55 eV larger in magnitude than for Cu. A Cu layer on Ag forms a potential barrier for thermalised positrons in the Ag substrate which then cannot freely diffuse to the surface. Also in the case when the evaporated material

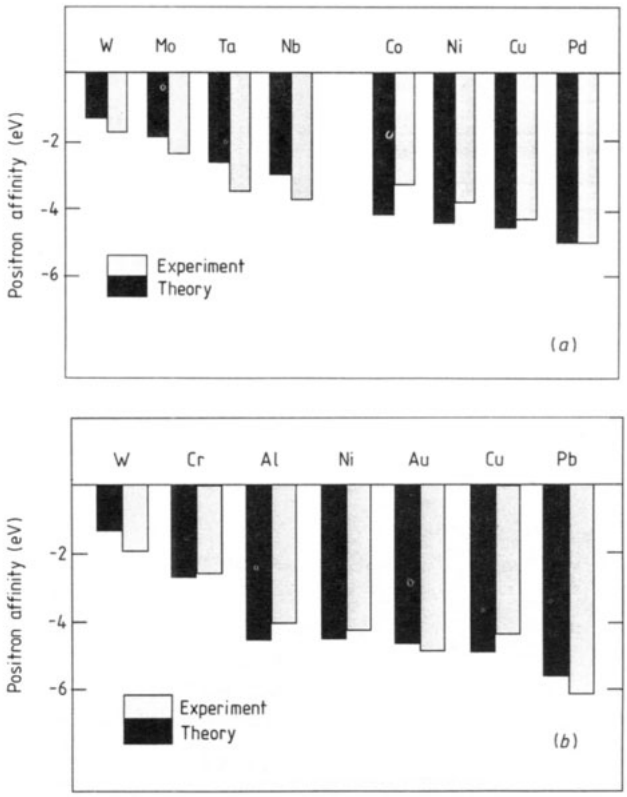

Figure 7. Comparison of the theoretical and experimental positron affinities. (*a*) The experimental values are measured directly by the reemitted-positron spectroscopy. (*b*) The experimental values are deduced from the measured positronium formation potentials by equation (6). For Al, Au, Cu, Ni, and Pb the experimental values are from [19], for Cr from [20], and for W from [21].

has a larger positron affinity in magnitude the potential step between different materials will cause wave-mechanical reflection of the positron and a reduction in the number of positrons reaching the surface. This effect should be manifest at low temperatures.

Another application of the positron affinity data is connected with the investigations of precipitates in the alloys by positron annihilation methods [23]. For example, aluminium alloys prepared by adding a few percent of Mg, Si, Cu, Zn, or Ag have been extensively studied. In these alloys precipitation process results in regions with a high concentration (over 50%) of the added element. Positrons are trapped by this kind of precipitates if they have a positron affinity larger in magnitude than the one for the bulk alloy. For the latter it is a good approximation to use the positron affinity for pure Al, because the dopant concentration is relatively low. In principle, the positron affinity for the precipitate should be calculated by using the actual lattice structure and composition of the precipitate, but already the value interpolated from the corresponding bulk material affinites is rather sufficient as will be discussed below. The main result is that the precipitate should be larger than a certain critical size in order for the trapping to occur. This size can be approximated from the calculated positron affinities: assuming that the precipitate can be described by a three-dimensional spherical potential well with

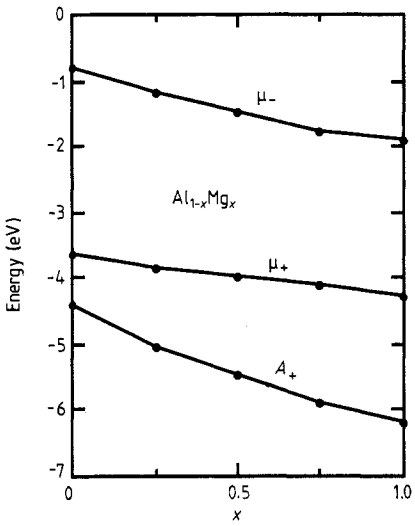

Figure 8. The electron (μ_-) and positron (μ_-) chemical potentials and the positron affinity (A_+) in $Al_{1-x}Mg_x$ as a function of the composition x. The FCC lattice structure with the lattice constant linearly interpolated from the values for pure Al and Mg metals is assumed in the calculations. The calculation is performed for the values $x = 0, 0.25, 0.5, 0.75$ and 1.0.

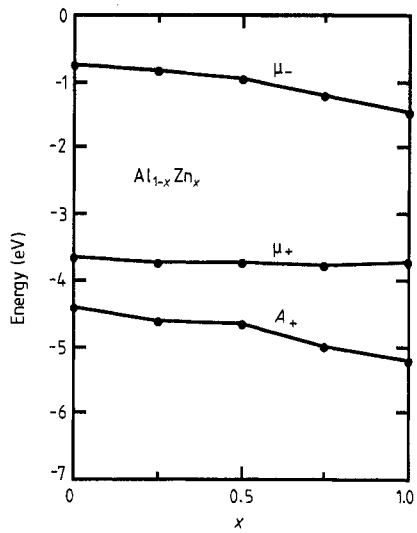

Figure 9. Same as figure 8 but for $Al_{1-x}Zn_x$.

the depth of the positron affinity difference ΔA, there is one bound state if the radius of the precipitate is larger than the critical radius

$$r_c \simeq 5.8\, a_0/\sqrt{\Delta A(\text{eV})}, \tag{11}$$

where a_0 is the Bohr radius. For example, if one applies this to the 100% Zn precipitates in Al, the critical radius is $5.4\, a_0$. This means that precipitates should contain at least ~6 Zn atoms.

In order to describe the precipitates more accurately, we have calculated the positron affinities for ordered $Al_{1-x}Mg_x$ and $Al_{1-x}Zn_x$ alloys as a function of the composition x. $Al_{1-x}Mg_x$ represents a case for which the atomic numbers of the constituents are nearly equal, but the lattice constants of the pure constituent metals are quite different. In the case of $Al_{1-x}Zn_x$ the situation is reverse i.e. the lattice constants are nearly equal, but the constituents belong to different rows of the Periodic table. In the calculations we have assumed the FCC-lattice for the alloy and the lattice constant is obtained by a linear interpolation from the pure metal lattice constants. The results are shown in figures 8 and 9. The changes in the positron affinity are determined mainly by the change in the electron chemical potential. In the case of the $Al_{1-x}Zn_x$ alloy the positron chemical potential is in fact nearly constant. The main result is that the positron affinity can be determined rather accurately by a linear interpolation. Moreover, an interesting detail given by the calculations is the positron distribution in the two different atomic spheres in the binary alloys. The spheres have equal radii. In the $Al_{1-x}Mg_x$ alloy positron is found with the same probability in the Al- and Mg-spheres, whereas in $Al_{1-x}Zn_x$ positron has a preference to Zn-spheres. For example, when $x = 0.5$ the probabilities are 53%

and 47% for the Zn- and Al-spheres, respectively. This tendency should be reflected e.g. in the measured core-annihilation contributions: because of the larger core size of Zn, the annihilation rate with the Zn-core electrons should be larger than that with Al-core electrons.

Stott and Kubica [22] have studied positron states in alloys by the positron pseudopotential method. Their approach is to some extent related to the present calculations. They studied the $x = 0.5$-alloys and calculated the positron pseudopotential differences between the constituent atoms in the alloy. The pseudopotential difference gives the positron preference for the one type of atom over the other type and it is related to the difference of the positron affinity for bulk materials defined in this paper. Namely, the pseudopotential differences calculated by Stott and Kubica consisted of three parts: (i) the difference in the Wigner–Seitz energy (~zero-point energy), (ii) the effects due to charge transfer between the different cells, which were approximated by the difference in the internal chemical potential for electrons in the two pure metals, (iii) the difference in the correlation potential were calculated using LDA with the average electron density in the cell of the pure metal. All the contributions were calculated using the average Wigner–Seitz radius of the atoms in the alloy. Using the calculated volume derivatives, our positron affinity values can be made to correspond to the average Wigner–Seitz radius of the alloy in question. The affinity differences obtained in this way agree qualitatively with the pseudopotential differences.

4. Conclusions

We have performed a systematic study of the ground state energetics for positrons in undefected elemental solids. The positron affinities calculated provide a consistent data base, which supports the interpretation of the experimental results obtained by the slow-positron-beam techniques or by the conventional positron annihilation methods. In this work we explain the trends seen in the positron affinities by the help of the variations of the electron and positron chemical potentials. The results are also compared with the available experimental values, and the agreement is good: the differences are less than ~10% of the total range of affinity values in different solids studied.

References

[1] For general reviews, see e.g. P Hautojärvi (ed.), 1979 *Positrons in Solids,* Springer Verlag, Berlin Heidelberg; W Brandt and A Dupasquier (ed.) 1983 *Positron Solid State Physics* (Amsterdam: North-Holland)
[2] For a review, see Schultz P J and Lynn K G 1988 *Rev. Mod. Phys.* **60** 701
[3] Lundqvist S and March N H ed. 1983 *Theory of the Inhomogeneous Electron Gas* (New York: Plenum)
[4] Andersen O K, Jepsen O and Glötzel D 1985 *Highlights of Condensed-Matter Theory* ed. F Basani, F Fumi and M P Tosi (Amsterdam: North-Holland) p 59
[5] Skriver H L 1984 *The LMTO Method* (New York: Springer)
[6] Vergés J A, Glötzel D, Cardona M and Andersen O K 1982 *Phys. Status Solidi* (b) **113** 519
[7] Lambrecht W R L and Segall B 1988 *Phys. Rev. Lett.* **61** 1764
[8] Boev O V, Puska M J and Nieminen R M 1987 *Phys. Rev.* B **36** 7786
[9] Ceperley D M and Alder B J 1980 *Phys. Rev. Lett.* **45** 566
Perdew J and Zunger A 1981 *Phys. Rev.* B **23** 5048
[10] Arponen J and Pajanne E 1979 *Ann. Phys., NY* **121** 343; 1979 *J. Phys. F: Met. Phys.* **9** 2359
[11] Puska M J, Mäkinen S, Manninen M and Nieminen R M 1989 *Phys. Rev.* B **39** 7666

[12] Bergersen B, Pajanne E, Kubica P, Stott M J and Hodges C H 1974 *Solid State Commun.* **15** 1377
[13] Bardeen J and Shockley W 1950 *Phys. Rev.* **80** 72
[14] Gullikson E M and Mills A P 1987 *Phys. Rev.* B **35** 8759
[15] Moruzzi V L, Janak J F and Williams A R 1978 *Calculated Electronic Properties of Metals* (New York: Pergamon)
[16] Nielsen B, Lynn K G and Vehanen A 1985 *Phys. Rev.* B **32** 2296
[17] Jorch H H, Lynn K G and MacKenzie I K 1981 *Phys. Rev. Lett.* **47** 362
Jorch H H, Lynn K G and McMullen T 1984 *Phys. Rev.* B **30** 93
[18] Gidley D W and Frieze W E 1988 *Phys. Rev. Lett.* **60** 1193
[19] Howell R H, Rosenberg I J, Fluss M J, Goldberg R E and Laughlin R B 1987 *Phys. Rev.* B **35** 5303
Howell R H, Rosenberg I J, Meyer P and Fluss M J 1987 *Phys. Rev.* B **35** 4555
[20] Wilson R J and Mills A P 1983 *Surf. Sci.* **128** 70
[21] Wilson R J 1983 *Phys. Rev.* B **27** 6974
[22] Huttunen P and Vehanen A unpublished
[23] For a review, see Dlubek G 1987 *Proc. of 4th Int. Conf. on Age-Hardenable Al-Alloys*, ed. I Kovács and J Lendvai (Materials Science Forum) **13–14** 11